https://doi.org/10.5194/essd-2026-866
Preprint. Discussion started: 4 November 2026
© Author(s) 2026. CC BY 4.0 License.



Open Access Earth System Science Data Discussions

A high-resolution dataset of pre-rainfall low-level vertical wind shear derived from radar wind profilers across China

Ning Li[a,b,c], Yongguang Zheng[c], Hui Xu[a,d], Tianmeng Chen[a,d], Xiaoran Guo[e], Linxi Zhao[a], Yuping Sun[a], Xuewei Cai[c], Honglong Yang[d], Liping Zeng[f], Jianping Guo[a,d,f*]

[a] *State Key Laboratory of Severe Weather Meteorological Science and Technology & Specialized Meteorological Support Technology Research Center, Chinese Academy of Meteorological Sciences, Beijing 100081, China*

[b] *College of Earth and Planetary Sciences, University of Chinese Academy of Sciences, Beijing 100049, China*

[c] *National Meteorological Centre, Beijing 100081, China*

[d] *CMA Field Scientific Experiment Base for Low-Altitude Economy Meteorological Support of Unmanned Aviation in Guangdong-Hong Kong-Macao Greater Bay Area, Shenzhen 518108, China*

[e] *Meteorological Observation Centre of China Meteorological Administration, Beijing 100081, China*

[f] *Guizhou New Meteorological Technology Co., Ltd, Guiyang, China,*

Correspondence to:

Dr./Prof. Jianping Guo (Email: jpguocams@gmail.com)

https://doi.org/10.5194/essd-2026-866
Preprint. Discussion started: 4 November 2026
© Author(s) 2026. CC BY 4.0 License.



Open Access Earth System Science Data Discussions

Abstract

Favorable low-level vertical wind shear (VWS) is an important dynamic feature conducive to rainfall development. However, continuous observations capable of resolving the fine-scale vertical structure and rapid pre-rainfall evolution of VWS remain limited. To address this observational gap, we developed a high-resolution low-level VWS dataset from wind measurements collected by a network of 28 radar wind profiler (RWP) stations across China during 2023–2025, with a focus on the 2 h preceding rainfall onset. The dataset provides bulk VWS for both the fixed 0.6–3.0 km layer and arbitrary combinations of vertical levels, local layer VWS, layer-mean VWS, maximum VWS, and the altitude of maximum VWS, with a temporal resolution of 6 min and a vertical resolution of 120 m over 0.6–4.08 km AGL. Comparison with collocated radiosonde measurements supports the reliability of the RWP-derived VWS, while comparison with ERA5 shows that the reanalysis underestimates localized maximum VWS and does not reproduce its rapid minute-scale evolution. Non-HR events are generally associated with stronger but relatively steady background VWS, whereas HR events show a pronounced nonlinear increase in local low-level VWS during approximately the final 30 min before rainfall onset. The latter is accompanied by an upward shift in the altitude of maximum VWS, indicating a redistribution of the strongest shear within the lower troposphere. These contrasting evolution patterns demonstrate the ability of the dataset to resolve transient and vertically localized changes in pre-rainfall dynamic environments that are not adequately represented by coarser-resolution reanalysis data. The dataset is publicly available at https://doi.org/10.5281/zenodo.23432237 (Li and Guo, 2026), which can serve as a valuable benchmark for diagnosing pre-rainfall dynamic environments to advance regional HR nowcasting. Accordingly, to realize such forecasting improvements, we must leverage fine-scale dynamic structures derived from RWP measurements for more complete characterizations of prestorm environments.

https://doi.org/10.5194/essd-2026-866
Preprint. Discussion started: 4 November 2026
© Author(s) 2026. CC BY 4.0 License.



Open Access Earth System Science Data Discussions

Short Summary

To better understand how winds change before rainfall, we created a unique dataset from 28 radar wind profiler stations across China. It captures wind shear every six minutes during the two hours before rainfall. Stronger rainfall is preceded by a rapid increase and vertical shift in shear, while lighter rainfall shows steadier conditions. The data reveal changes missed by widely used weather analyses and may help improve short-term rainfall forecasts.

https://doi.org/10.5194/essd-2026-866
Preprint. Discussion started: 4 November 2026
© Author(s) 2026. CC BY 4.0 License.



1. Introduction

Accurate nowcasting of regional heavy rainfall (HR) remains a major challenge in operational meteorology (Trier et al., 2006), owing in part to incomplete characterization of the pre-rainfall environment, limited continuous high-resolution observations, and limitations in model parameterizations (Carbone and Tuttle, 2008; Reif and Bluestein, 2017; Fitzpatrick et al., 2020). An important aspect of this challenge is resolving the fine-scale structure of the boundary layer and lower troposphere, which can exert a strong influence on convective initiation and organization. Low-level vertical wind shear (VWS), typically defined as the change of the wind vector or one of its components with height (Glickman, 2000), is therefore an important dynamical characteristic of convective environments (e.g., Rotunno et al., 1988; Coniglio et al., 2006).

Extensive research has shown that the magnitude, orientation, and altitude of low-level VWS interact with convection in complex ways (Stensrud et al., 2005; Hande et al., 2012). These interactions can modulate storm inflow (Alfaro, 2017), updraft buoyancy (Mulholland et al., 2021), and the organization and longevity of thunderstorms (Fovell and Ogura, 1989; Taylor et al., 2017; Barton et al., 2025). The interaction between low-level environmental shear and cold-pool-generated circulation is central to the RKW conceptual framework for squall-line organization (Rotunno et al., 1988), although convective-system responses also depend on thermodynamic and environmental conditions. Low-level VWS has also been associated with variations in the probability and intensity of extreme precipitation (Taylor et al., 2026), and localized shear maxima have been reported shortly before some HR events (Zheng and Sun, 2016). Barton et al. (2025) further showed enhanced positive shear anomalies immediately preceding storm occurrence. Collectively, these findings indicate that VWS should be considered not only as a background environmental property but also as a quantity that can exhibit pronounced temporal and vertical variability before convective events. Accurately characterizing the fine-scale vertical structure of low-

https://doi.org/10.5194/essd-2026-866
Preprint. Discussion started: 4 November 2026
© Author(s) 2026. CC BY 4.0 License.

Open Access Earth System Science Data Discussions

level VWS and its evolution preceding rainfall is therefore important for understanding pre-convective dynamical environments and improving nowcasting capabilities.

Despite these advances, the continuous evolution of low-level VWS immediately preceding rainfall remains insufficiently characterized. Previous studies have relied on a combination of reanalysis products (Aiyyer and Thorncroft, 2006), numerical simulations (Frank and Ritchie, 2001; Draxl et al., 2014; Maybee et al., 2024), radiosonde measurements (Houchi et al., 2010; Ko and Chun, 2026), and radar observations (Augros et al., 2013) to examine VWS climatology, large-scale variability, and convective environments. Each of these data sources has limitations for resolving rapid, vertically localized changes in VWS immediately before rainfall. Conventional radiosondes typically provide only two soundings per day; commercial aircraft reports, although providing direct wind measurements, remain spatially and temporally sparse because of flight-route and altitude constraints (Lin et al., 2021); and Doppler wind lidars are often used for localized wind and wind-shear monitoring, particularly around airports (Xue et al., 2026). Reanalysis products and numerical models provide favorable spatiotemporal continuity but may not resolve fine-scale features such as low-level jets (LLJs), sharp boundary-layer gradients, and highly localized extreme shear structures (Houchi et al., 2010). Because convective environments can undergo rapid dynamical adjustments from hours to minutes before rainfall initiation, these limitations hinder systematic investigation of minute-scale VWS evolution during the critical pre-rainfall window.

Ground-based radar wind profilers (RWPs) can address several of these limitations by continuously acquiring vertical wind profiles at minute-scale temporal and hectometer-scale vertical resolutions. Their observations enable rapid low-level wind adjustments to be tracked as precipitation systems approach (Zamora et al., 1987; Molod et al., 2019; Guo et al., 2023; Li et al., 2024). Leveraging the national RWP network established in China since 2008 (Guo et al., 2021), recent studies have demonstrated the potential of RWP observations for resolving rapidly evolving pre-rainfall atmospheric dynamics (Chen et al., 2024), including rapid intensification of LLJs within 30 min of nocturnal rainfall onset (Li et al., 2026). However, this

https://doi.org/10.5194/essd-2026-866
Preprint. Discussion started: 4 November 2026
© Author(s) 2026. CC BY 4.0 License.



observational capability has not yet been translated into a standardized data product specifically designed to characterize the continuous evolution of pre-rainfall VWS across China.

Against this background, this study uses observations from the RWP network in China to construct a high-resolution dataset of low-level VWS spanning 2023–2025, with a specific focus on the 2 h preceding rainfall onset. The resulting dataset provides an observational basis for systematically characterizing pre-rainfall VWS across China and for evaluating the representation of fine-scale wind-shear structures in reanalysis and numerical weather prediction products. The remainder of the paper is organized as follows: Sect. 2 describes the datasets and calculation methodology, Sect. 3 evaluates the dataset and characterizes pre-rainfall VWS variability, Sect. 4 describes data availability, and Sect. 5 summarizes the main findings and limitations.

2. Data and Methodology

2.1 Radar wind profiler measurements

The RWP observations collected from 28 stations across China (Table 1 and Fig. 1a) during 2023–2025 were utilized to construct the high-resolution VWS dataset. These RWPs continuously provide vertical profiles of horizontal wind speed and direction at an interval of 6 min (Liu et al., 2019). To ensure vertical consistency across all stations, all profiles were interpolated to a uniform vertical resolution of 120 m, starting at 0.12 km above ground level (AGL).

The RWPs detect vertically resolved wind fields by transmitting and receiving electromagnetic beams in five directions, comprising a zenith beam and four inclined beams at 15° zenith angles towards the east, south, west, and north, respectively. By analyzing the Doppler shifts in radial velocities from any three beams, the horizontal and vertical wind components are retrieved. However, falling hydrometeors (e.g., raindrops) and other particulate scatterers may introduce biases in radar measurements, thereby contaminating the horizontal wind retrievals (Angevine, 1997; Wang et al.,

https://doi.org/10.5194/essd-2026-866
Preprint. Discussion started: 4 November 2026
© Author(s) 2026. CC BY 4.0 License.



150 2014). To minimize such precipitation-induced contamination, all RWP observations
151 recorded during rainfall periods were strictly excluded from the dataset.

152 **Table 1.** Radar wind profiler stations used in this study

Station ID	Station Name	Lon. (°)	Lat. (°)	Altitude (m)
51839	Minfeng	82.69	37.07	1408.90
52533	Jiuquan	98.49	39.77	1477.20
53463	Hohhot	111.57	40.86	1152.10
53772	Taiyuan	112.58	37.62	785.00
53845	Yan'an	109.45	36.58	1180.40
54304	Zhangjiakou	115.27	40.95	726.00
54342	Shenyang	123.51	41.73	50.00
54511	Beijing	116.47	39.81	31.50
54727	Zhangqiu	117.52	36.65	251.90
55664	Tingri	87.12	28.65	4326.80
56029	Yushu	96.96	33.00	3684.00
56146	Ganzi	100.00	31.62	3353.00
56173	Hongyuan	102.55	32.79	3465.00
56312	Linzhi	94.36	29.65	2988.40
56651	Lijiang	100.22	26.85	2382.40
56964	Simao	100.99	22.82	1423.30
57461	Sanxia	111.36	30.74	253.80
57516	Chongqing	106.46	29.58	260.00
57687	Changsha	112.79	28.11	46.00
57816	Guiyang	106.73	26.59	1223.70
58238	Nanjing	118.90	31.93	40.60
58459	Hangzhou	120.29	30.18	43.00
58633	Quzhou	118.89	28.99	86.40
58725	Shaowu	117.50	27.31	363.60
58847	Fuzhou	119.29	26.08	112.10
59312	Chaozhou	116.69	23.67	7.00
59431	Nanning	108.55	22.78	104.90
59758	Haikou	110.25	19.99	69.00

153

https://doi.org/10.5194/essd-2026-866
Preprint. Discussion started: 4 November 2026
© Author(s) 2026. CC BY 4.0 License.



Data availability was assessed for all horizontal wind profiles throughout 2023–2025. As shown in Figs. 1b and 1c, overall data availability is high, although the data recovery rate is relatively low at high altitudes, likely attributed to the inherent signal attenuation of the radar. Within the effective altitude range of 0.6–4.08 km AGL, mean data availability exceeded 85% across all stations, supporting the temporal continuity required for the VWS analysis.

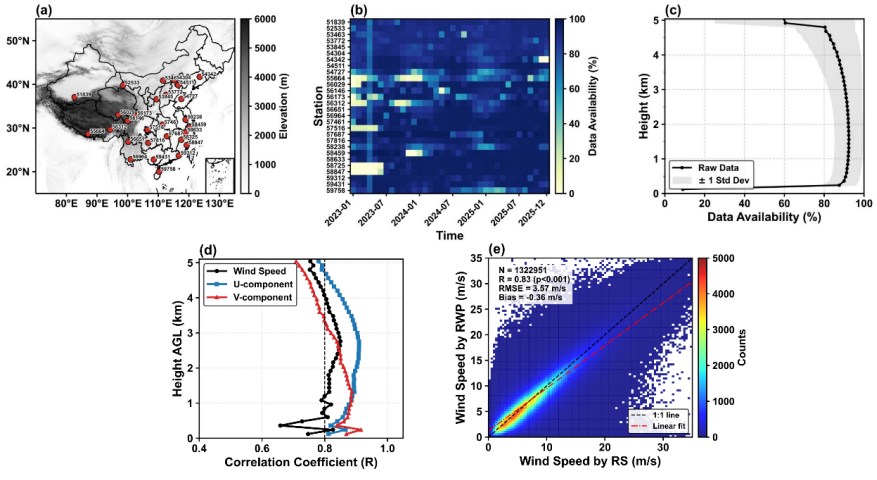


Figure 1. (a) Spatial distribution of the 28 Radar Wind Profiler (RWP) stations (red dots) overlaid on terrain elevation across China. (b) Temporal variation of data availability for all RWP stations listed in Table 1 during 2023–2025. (c) Vertical profile of the national mean data availability, with the gray shading indicating the ±1 standard deviation. (d) Vertical profiles of the correlation coefficient (R) between the RWP stations and upper-air radiosonde (RS) measurements for horizontal wind speed, as well as zonal (U) and meridional (V) wind components. (e) Density scatterplot of matched wind-speed observations from RWP versus RS at altitudes ranging from 0.6 to 4.08 km above ground level (AGL). Red and black dashed lines denote the linear regression fit and the 1:1 reference line, respectively.

https://doi.org/10.5194/essd-2026-866
Preprint. Discussion started: 4 November 2026
© Author(s) 2026. CC BY 4.0 License.



2.2 Evaluation of horizontal winds of the RWP

To further evaluate RWP data quality, horizontal wind speed and its zonal and meridional components were compared with coincident radiosonde (RS) observations at corresponding stations and altitude levels. Radiosonde measurements provide an independent reference for evaluating ground-based remote-sensing wind retrievals. Sounding balloons are launched twice daily at 08:00 and 20:00 local standard time (LST), providing vertical profiles of temperature, pressure, relative humidity, and horizontal wind at a vertical resolution of approximately 5–8 m. During summer (June–August), additional soundings at 14:00 LST were conducted at most radiosonde stations in China.

The RWP-derived horizontal winds, including the U and V components, show strong positive correlations with radiosonde observations, with correlation coefficients (R) exceeding 0.8 throughout the 0.6–4.08 km AGL layer (Fig. 1d). Measurements below 0.5 km were less reliable because of near-surface clutter. The pooled comparison across 0.6–4.08 km AGL yields R = 0.83 (Fig. 1e). These results support the use of RWP-derived horizontal winds within this altitude range; accordingly, the effective vertical range of the VWS dataset was restricted to 0.6–4.08 km AGL.

2.3 Multi-source meteorological data

Minute-level rainfall data were directly acquired from the rain gauge measurements at national weather stations co-located with the RWPs across China. To ensure strict temporal alignment with the RWP measurements, rainfall amounts were accumulated over 6-min intervals. These observations underwent rigorous quality control (China Meteorological Administration, 2020; Zhao et al., 2024) and are publicly accessible at the National Meteorological Information Center of China Meteorological Administration (CMA).

Furthermore, the fifth generation of the European Centre for Medium-Range Weather Forecasts atmospheric reanalysis (ERA5) of the global climate (Hersbach et al., 2020) was used to calculate reanalysis-derived VWS and compare it with RWP-

https://doi.org/10.5194/essd-2026-866
Preprint. Discussion started: 4 November 2026
© Author(s) 2026. CC BY 4.0 License.



derived VWS before rainfall onset. ERA5 data provide hourly atmospheric fields, including zonal wind, meridional wind, and geopotential height, on a 0.25° × 0.25° grid with 37 vertical pressure levels (Hersbach et al., 2020). For each rainfall event, ERA5 data within 2 h prior to rainfall were sampled, and the VWS was calculated using the grid points nearest to each RWP station. This station-based approach enabled direct comparisons between reanalysis and RWP observations rather than performing a domain-wide average across the entire study region (Ko and Chun, 2026). Unless otherwise specified, all datasets cover the period 2023–2025.

2.4 Identification of rainfall events

To isolate pre-rainfall environments, rainfall events were required to be separated by a minimum dry interval of 2 h. Rainfall onset was defined as the first 6 min interval in which accumulated rainfall at the corresponding RWP station exceeded 0.1 mm. To account for rainfall intermittency and filter transient noise, a valid rainfall event required the initial detection to be followed by at least two additional rainfall occurrences within the subsequent 30 min. Any isolated initial occurrence not meeting this criterion was discarded.

Rainfall events were further classified by intensity to examine systematic differences between HR and non-HR events. Following Li et al. (2026), localized HR events were defined as those for which the mean 6 min rainfall intensity exceeded the station-specific 75th percentile of all recorded rainfall events. This percentile-based definition identifies relatively intense events at each station while retaining a sufficient sample size for statistical analysis of minute-scale VWS dynamics. Here, “HR” denotes the upper quartile of event intensity at each station and should not be interpreted as the operational heavy-rainfall threshold used by CMA. The final sample comprised 10,950 rainfall events during 2023–2025, of which 2,705 were classified as HR events.

2.5 Calculation of VWS

Four VWS metrics were calculated: bulk VWS, layer VWS, mean VWS, and maximum VWS (max VWS). Bulk VWS was defined as:

https://doi.org/10.5194/essd-2026-866
Preprint. Discussion started: 4 November 2026
© Author(s) 2026. CC BY 4.0 License.



Open Access Earth System Science Data Discussions

$$bulk\ VWS=\frac{\sqrt{(u_{top}-u_{bottom})^2+(v_{top}-v_{bottom})^2}}{\Delta z} \quad (1)$$

where z is the altitude and u and v represent the zonal and meridional wind components, respectively. This definition quantifies the magnitude of the vector wind difference between two altitude levels (Zhang et al., 2020). Bulk VWS between 0.6 and 3.0 km AGL was also calculated to provide a conventional layer-shear metric for comparison with ERA5-derived VWS.

To characterize fine-scale vertical shear variability, local layer VWS was calculated using a centered finite-difference approach based on horizontal wind vectors at two vertically separated levels. The corresponding mean VWS was obtained by averaging the valid local shear values over the 0.6–4.08 km above-ground-level (AGL) profile:

$$layer\ VWS=\sqrt{\left(\frac{u_{i+1}-u_{i-1}}{z_{i+1}-z_{i-1}}\right)^2+\left(\frac{v_{i+1}-v_{i-1}}{z_{i+1}-z_{i-1}}\right)^2} \quad (2)$$

$$mean\ VWS=\frac{1}{N}\sum_{i=1}^{N} layer\ VWS \quad (3)$$

where u and v are the zonal and meridional wind components, respectively; i is the vertical index and N is the number of valid local shear estimates within the analyzed profile. Unlike bulk VWS, which depends only on wind vectors at the selected layer boundaries, mean VWS characterizes the average magnitude of local shear throughout the vertical profile (Ko and Chun, 2026).

Finally, we defined max VWS as the maximum local layer shear within the same altitude profile:

$$max\ VWS=max\ (layer\ VWS) \quad (4)$$

The corresponding altitude of max VWS was defined as the midpoint of the two levels used to calculate the maximum local shear. This metric identifies the strongest localized shear within the profile and enables the temporal evolution of extreme shear values before rainfall onset to be examined.

https://doi.org/10.5194/essd-2026-866
Preprint. Discussion started: 4 November 2026
© Author(s) 2026. CC BY 4.0 License.



3. Results and discussion

3.1 Validation and Statistical Characteristics of VWS

To evaluate the reliability of the RWP-derived VWS dataset, the derived shear metrics were compared with collocated RS measurements. Overall, the RWP-derived VWS shows good agreement with the RS estimates in both magnitude and vertical structure. Figures 2a and 2b show a representative case at the Beijing station. The RWP captures fine-scale vertical fluctuations in both horizontal wind components and the resulting VWS, with close correspondence to the collocated RS profiles. In this example, strong-shear layers near approximately 1.0 and 2.5 km are evident in both datasets, and only small differences are found in maximum VWS and 0.6–3.0 km bulk VWS.

Statistically, median VWS profiles aggregated from all matched samples during 2023–2025 show close agreement between the two observing systems across 0.6–4.08 km AGL, with the median bias remaining near zero (Fig. 2c). Enhanced shear within approximately 0.8–1.4 km AGL may be associated with boundary-layer processes, including surface-friction effects and vertical gradients near the PBL top. The distribution of maximum VWS was also evaluated because localized shear extrema are relevant to convective environments. As shown in Fig. 2d, the RWPs reproduce the main distributional features observed by RS, including a bimodal distribution in the altitude of maximum VWS. The lower-altitude mode (0.6–1.0 km) may be associated with shear near the frictional boundary layer or PBL top, whereas the higher-altitude mode (2.5–3.5 km) may reflect elevated shear associated with LLJs or frontal structures. Although the RWP distribution shows a slight positive skew in maximum-VWS magnitude and a slight downward shift in its occurrence height relative to RS, the overall distributional features are broadly preserved.

https://doi.org/10.5194/essd-2026-866
Preprint. Discussion started: 4 November 2026
© Author(s) 2026. CC BY 4.0 License.

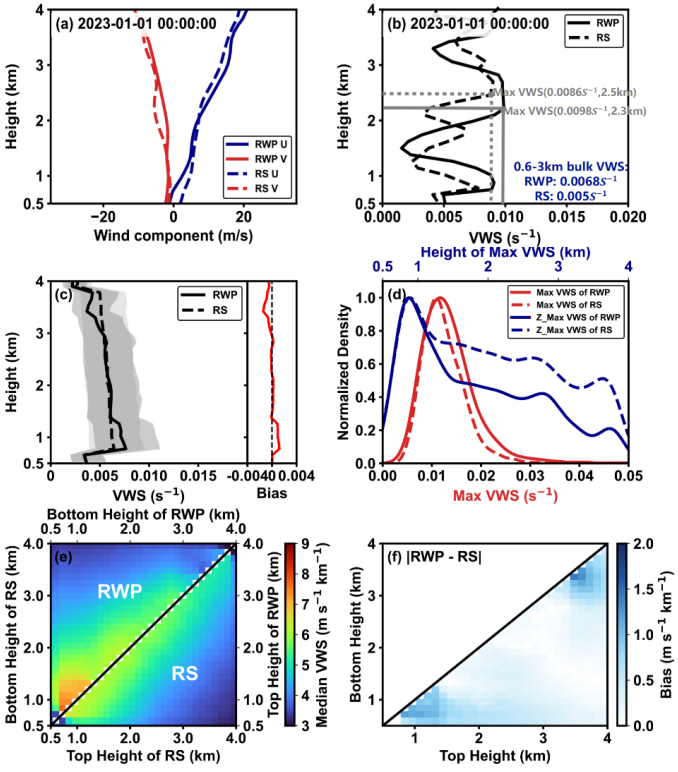


Figure 2. (a) Vertical profiles of zonal (U, blue lines) and meridional (V, red lines) wind components sampled at the Beijing station at 08:00 LST on 1 January 2023, and (b) corresponding vertical profiles of the layer VWS from RWP (solid lines) and RS (dashed lines) observations. (c) Median VWS profiles (0.6–4.08 km) across all stations spanning 2023–2025. The gray shaded envelope represents the interquartile range (25th to 75th percentiles). The right subpanel displays the median bias (RWP minus RS). (d) Normalized probability density functions (PDFs) of the max VWS (red lines) and its corresponding height (blue lines). (e) Split-diagonal heatmap of median bulk shear (10^{-3} s^{-1}) calculated across varying bottom and top boundary heights. RWP and RS observations are displayed in the upper-left and lower-right triangles, respectively. (f) Absolute bulk shear bias (|RWP − RS|), shown exclusively in the valid lower-right triangle (top > bottom height).

https://doi.org/10.5194/essd-2026-866
Preprint. Discussion started: 4 November 2026
© Author(s) 2026. CC BY 4.0 License.



To evaluate the dataset across a range of layer depths, bulk shear was compared between arbitrary pairs of height boundaries (Fig. 2e). The close structural agreement between the RWP (upper-left) and RS (lower-right) triangles indicates consistency across different layer depths. The absolute-bias matrix (Fig. 2f) further shows small bulk-shear differences across most height combinations. Slight deviations below 1.5 km and above 3.5 km may partly reflect differences in sampling characteristics: the RS balloon experiences wind-induced horizontal drift, whereas the RWP performs vertically fixed-point profiling. In addition, because VWS is derived from vertical differences in horizontal wind, shear estimates can amplify small high-frequency measurement errors. Overall, the quantitative and structural agreement supports the reliability of the RWP-derived VWS dataset.

Building on the validated dataset, we characterized the shear environments during the 2 h preceding HR and non-HR events (Fig. 3). Non-HR events show a higher probability of occurring under stronger VWS conditions. Specifically, the occurrence peaks of layer-mean and maximum VWS from the RWPs are larger for non-HR events than for HR events (Figs. 3b and 3c). In addition, the altitude of maximum VWS for non-HR events is more strongly concentrated in the lower boundary layer (Fig. 3d). These distributions indicate that background VWS magnitude alone does not distinguish HR from non-HR events.

Although the ERA5 reanalysis (dashed lines) can capture the general distinction between HR and non-HR events, it tends to overestimate the bulk VWS while systematically underestimating the fine-scale VWS metrics, including the layer-mean VWS, max VWS and its occurrence height. Furthermore, the distribution of max VWS altitude derived from ERA5 is predominantly unimodal, with most values concentrated below 1 km. In contrast, the high-resolution RWP data effectively resolve the vertically layered and highly localized dynamic structures, including fine-scale shear features that are not adequately represented by ERA5. The difference highlights the inherent limitations of coarse-resolution reanalysis products in representing transient, extreme

https://doi.org/10.5194/essd-2026-866
Preprint. Discussion started: 4 November 2026
© Author(s) 2026. CC BY 4.0 License.



dyanmic structures preceding rainfall, thereby underscoring the added value of the RWP observations for resolving fine-scale VWS environments.

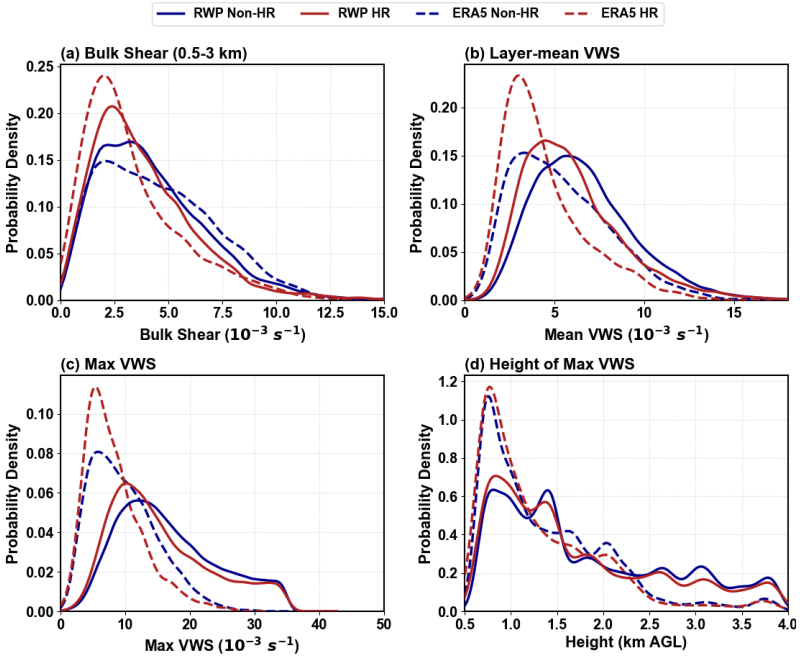


Figure 3. PDFs of (a) 0.6–3.0 km bulk VWS, (b) layer-mean VWS, (c) maximum VWS, and (d) the altitude of maximum VWS during the 2 h preceding non-HR (blue) and HR (red) events. Solid lines represent RWP observations, and dashed lines represent ERA5 reanalysis data.

3.2 Vertical Structure of VWS preceding rainfall

To elucidate the contrasting precursor characteristics of VWS across rainfall-intensity categories, this section examines the fine-scale vertical evolution of VWS during the 2 h preceding rainfall onset. The results show that rapid structural adjustment of VWS, rather than background magnitude alone, is associated with subsequent rainfall intensity.

The temporal redistribution of VWS probabilities as rainfall approaches is captured via Normalized Contoured Frequency by Altitude Diagrams (NCFADs; Fig.

https://doi.org/10.5194/essd-2026-866
Preprint. Discussion started: 4 November 2026
© Author(s) 2026. CC BY 4.0 License.



4). For non-HR events (Fig. 4a–c), the overall vertical VWS distribution remains relatively stable throughout the 2 h period. Although the frequency of high VWS values increases slightly during the final 30 min, the RWP-derived mean profiles (black lines) remain nearly unchanged, indicating limited pre-onset adjustment of the vertical wind-shear structure. In stark contrast, HR events are characterized by a systematic rightward shift in the VWS probability distribution (Fig. 4d–f). During the final [-30, 0) min window (Fig. 4f), the frequency of weak shear decreases markedly (blue shading), whereas strong shear becomes substantially more frequent (red shading), particularly in the lower troposphere. This rapid enhancement of low-level shear constitutes a distinct pre-onset dynamic signature of HR events in the composite analysis. Crucially, while the RWP-derived profiles capture the rapid intensification of local VWS, the corresponding ERA5 profiles remain temporally static, missing the rapid change of low-level wind field immediately preceding rainfall onset. This contrast highlights the importance of high-resolution RWP observations for resolving transient and vertically localized shear structures preceding intense rainfall.

The relatively weak VWS observed during the early stages preceding HR does not necessarily indicate an unfavorable environment for intense precipitation, as rainfall intensity depends on the combined effects of environmental shear, thermodynamic instability, moisture, and mesoscale forcing. The subsequent rapid intensification of low-level VWS may reflect evolving vertical gradients in horizontal momentum associated with mesoscale circulations or LLJs, potentially favoring convective organization under supportive thermodynamic conditions. Thus, this result suggests that the rapid evolution and vertical redistribution of shear may provide additional information beyond background shear magnitude alone for distinguishing HR from non-HR environments.

https://doi.org/10.5194/essd-2026-866
Preprint. Discussion started: 4 November 2026
© Author(s) 2026. CC BY 4.0 License.

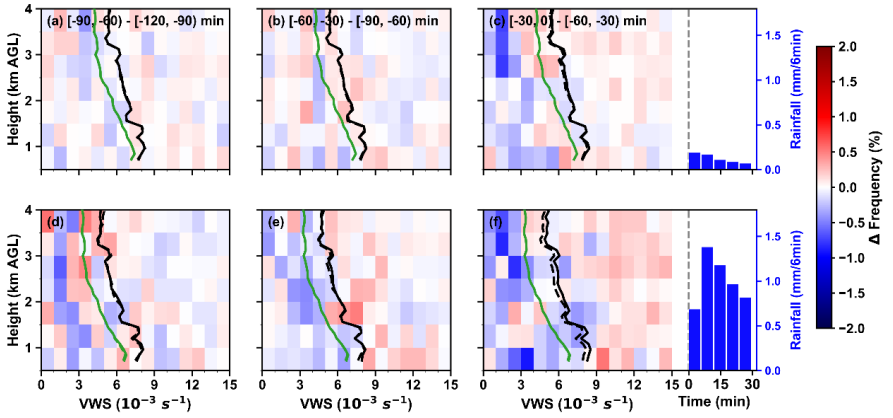


Figure 4. Differences in normalized contoured frequency by altitude diagrams (NCFADs) for layer VWS between adjacent 30 min windows preceding the onset of non-HR events: (a) [-90, -60) minus [-120, -90) min, (b) [-60, -30) minus [-90, -60) min, and (c) [-30, 0) minus [-60, -30) min, where 0 min corresponds to the rainfall onset. Overlaid profiles show the mean VWS derived from RWP observations (black) and ERA5 reanalysis (green). For each panel, solid and dashed lines represent the current and preceding time windows, respectively, with the ERA5 profiles based on the corresponding hourly analysis times. Red (blue) shading indicates an increase (decrease) in normalized frequency. In panels (c) and (f), blue bars show the temporal evolution of rainfall intensity (mm per 6 min) during the first 30 min following rainfall onset.

To further examine the statistical redistribution of shear structures, the temporal differences in composite bulk VWS are presented in Fig. 5 across all layer combinations. For non-HR events, positive shear changes are localized and discontinuous (Figs. 5a–c), indicating heterogeneous pre-rainfall shear enhancement across layer combinations. Even immediately before onset, the positive changes remain confined to a limited subset of lower–upper boundary combinations rather than forming a coherent enhancement across a broad range of layer depths. In contrast, HR events exhibit a pronounced and rapid enhancement of VWS. Following relatively weak changes during the earliest pre-onset interval (Fig. 5d), a systematic intensification emerges

https://doi.org/10.5194/essd-2026-866
Preprint. Discussion started: 4 November 2026
© Author(s) 2026. CC BY 4.0 License.



approximately 1 h before rainfall onset (Fig. 5e), with the strongest positive changes occurring during the final 30 min (Fig. 5f).

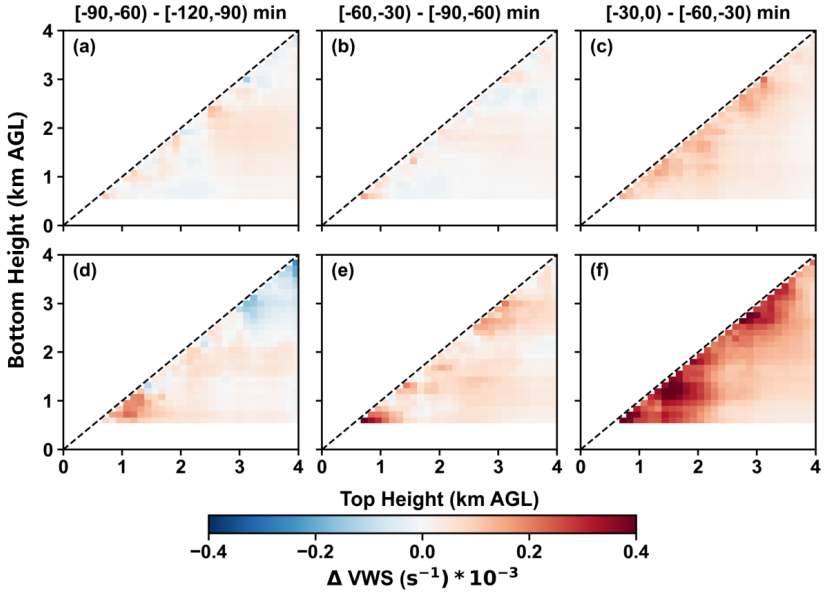


Figure 5. As in Fig. 4, but showing differences in composite bulk vertical wind shear (VWS; shading, 10^{-3} s^{-1}) between consecutive 30 min windows. The horizontal and vertical axes represent the upper and lower boundary heights (km AGL), respectively, used to calculate bulk VWS for each height pair. Warm (cold) colors indicate an increase (decrease) in composite bulk VWS between the corresponding time windows.

The intensification is concentrated mainly in the lower troposphere (below 2.0 km AGL), while enhanced shear also appears across progressively deeper layer combinations extending toward 2.5–3.5 km. This pattern indicates a vertical redistribution of shear before HR onset, although the observations alone do not establish the underlying dynamical mechanism. Such changes may alter the dynamic environment for storm inflow and convective organization, but their direct contribution to rainfall intensification requires further investigation.

https://doi.org/10.5194/essd-2026-866
Preprint. Discussion started: 4 November 2026
© Author(s) 2026. CC BY 4.0 License.



Taken together, the contrasting evolution of VWS suggests that rapid intensification and vertical redistribution are more strongly associated with HR events than the presence of strong background shear alone. These transient, vertically localized features are resolved by the RWP-derived dataset but are less evident in the reanalysis, highlighting the value of high-resolution wind-profile observations for characterizing pre-rainfall dynamic environments.

3.3 Minute-scale continuous evolution of VWS preceding rainfall

Figure 6 tracks the continuous minute-scale evolution of VWS and the corresponding composite hodographs preceding rainfall. At the beginning of the 2 h pre-onset period, the 0.6–3.0 km bulk shear, layer-mean VWS, and maximum VWS are generally stronger for non-HR events (blue) than for HR events (red), but the non-HR metrics vary only modestly thereafter. In contrast, HR events exhibit a steep nonlinear intensification in layer-mean and maximum VWS beginning approximately 30 min before onset. During this final 30 min, maximum VWS increases sharply and reaches its highest composite value near rainfall onset. Non-HR events also show gradual increases from approximately −30 min, but these changes are much smaller. Thus, the principal distinction between the two groups lies in the temporal evolution of local shear rather than in the absolute magnitude of background shear.

https://doi.org/10.5194/essd-2026-866
Preprint. Discussion started: 4 November 2026
© Author(s) 2026. CC BY 4.0 License.

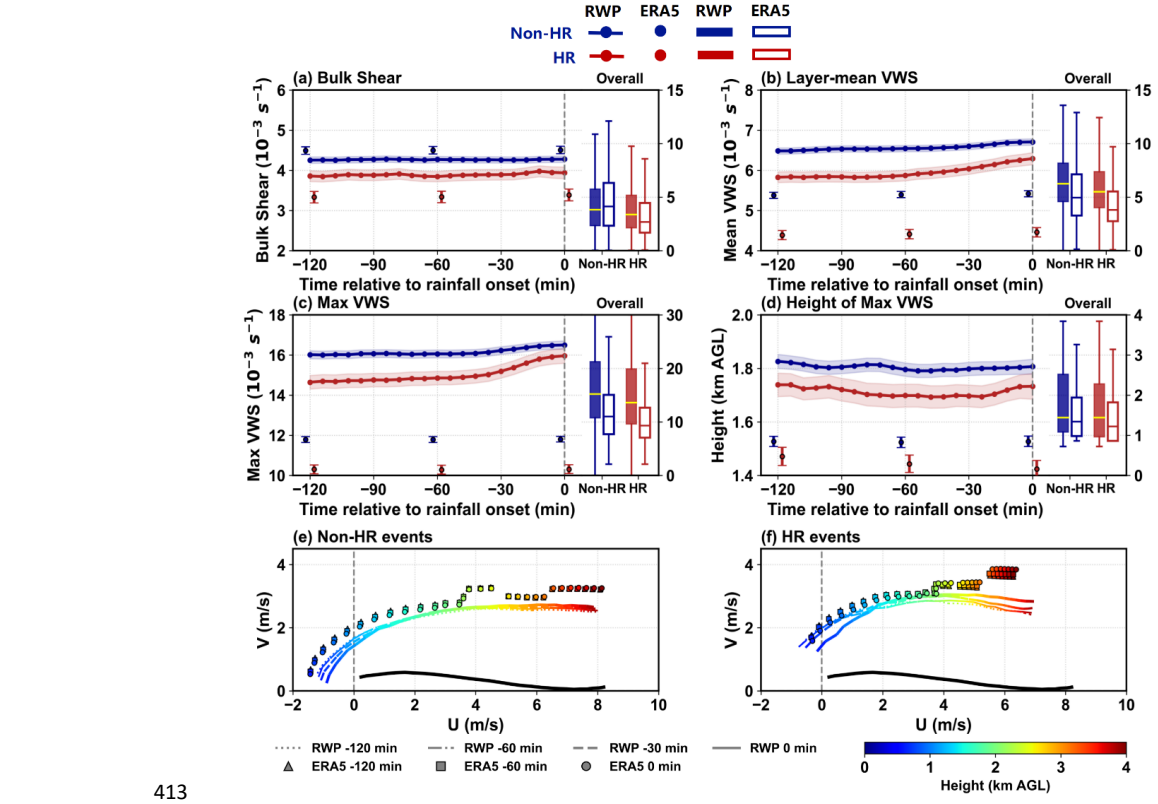


Figure 6. Temporal evolution of low-level VWS and composite hodographs preceding rainfall onset for non-HR (blue) and HR (red) events. (a–d) Evolution of (a) 0.6–3.0 km bulk VWS, (b) layer-mean VWS, (c) maximum VWS, and (d) the altitude of maximum VWS during the 2 h preceding rainfall onset. Solid lines and symbols represent radar wind profiler (RWP) observations and ERA5 reanalysis, respectively, with shaded envelopes and error bars indicating the corresponding 95 % confidence intervals. The boxplots on the right show the distributions of each variable over the 2 h pre-onset period. (e, f) Composite hodographs preceding (e) non-HR and (f) HR events, with the solid black line representing the climatological mean hodograph for 2023–2025.

Furthermore, the enhancement of pre-rainfall wind shear exhibits pronounced vertical heterogeneity. In contrast to the abrupt increase in maximum VWS, the broad 0.6–3.0 km bulk VWS shows little variation, indicating that the rapid intensification is

https://doi.org/10.5194/essd-2026-866
Preprint. Discussion started: 4 November 2026
© Author(s) 2026. CC BY 4.0 License.



concentrated within specific altitude layers. For HR events, the altitude of maximum VWS shows a two-stage evolution before rainfall onset. From −120 to approximately −30 min, its mean altitude decreases from approximately 1.74 to 1.68 km AGL (Fig. 6d), indicating that the strongest local shear becomes progressively concentrated at lower levels. The present observations do not distinguish whether this shift results from vertical momentum transport, changes in the background wind profile, or evolving mesoscale circulations. After approximately −30 min, the altitude of maximum VWS shifts upward, reaching about 1.73 km by rainfall onset. This upward tendency coincides with the increase in maximum VWS (Fig. 6c), indicating a simultaneous change in both the magnitude and vertical position of the strongest local shear. Compared with the weaker and more irregular variations in non-HR events, HR events therefore exhibit a distinct final-stage reorganization of the VWS profile. This pattern represents an observed dynamic feature associated with the final pre-onset stage of HR events rather than direct evidence of a causal triggering mechanism.

To further examine the evolution of the vertical wind structure, composite hodographs were analyzed (Figs. 6e and 6f). Compared with the non-rainfall climatological background (solid black line), the low-level wind vectors preceding rainfall exhibit clockwise turning with height. The hodographs reveal marked differences in wind-profile structure and temporal evolution between the two rainfall types, with potential implications for convective organization (Markowski and Richardson, 2007). For non-HR events (Fig. 6e), the hodograph is elongated predominantly along the zonal wind (U) axis, with the U component reaching approximately 8.0 m s^{-1}, but it exhibits relatively weak curvature, especially above 2 km AGL, indicating primarily unidirectional shear. Over the 2 h pre-onset period, the hodograph changes only slightly, with the meridional wind (V) component remaining near 2.5 m s^{-1}. In contrast, HR events (Fig. 6f) exhibit greater hodograph curvature and thus stronger directional shear; however, storm-relative quantities cannot be inferred without information on storm motion. As rainfall onset approaches, the HR hodographs progressively extend along the V axis, with the meridional wind component increasing

https://doi.org/10.5194/essd-2026-866
Preprint. Discussion started: 4 November 2026
© Author(s) 2026. CC BY 4.0 License.



455 from approximately 2.8 to 3.2 m s^{-1}. This expansion indicates a rapid adjustment of the
456 low-level wind field, particularly its meridional component, consistent with the
457 localized shear intensification in Figs. 6b and 6c. These changes may modify the
458 vertical distribution of horizontal vorticity and the dynamic environment for developing
459 convection, but their contribution to storm-relative helicity and convective dynamics
460 cannot be quantified from the composite hodographs alone.

461 Compared with RWP observations, the ERA5 reanalysis exhibits systematic
462 differences in its representation of the fine-scale wind shear structure and temporal
463 evolution preceding rainfall. As shown in Figs. 6a–d, while ERA5 broadly reproduces
464 the magnitude of 0.6–3.0 km bulk VWS, it substantially underestimates max VWS.
465 Specifically, ERA5-derived maximum VWS is approximately 30–35 % lower than the
466 RWP-derived values, with ERA5 estimates of 10.4–11.8 × 10^{-3} s^{-1}, and the altitude of
467 max VWS is biased downward by approximately 0.3 km. The ERA5-derived
468 hodographs reproduce some aspects of the enhanced meridional flow associated with
469 HR events but exhibit much weaker temporal variations than those resolved by the
470 RWPs. Consequently, although ERA5 provides useful information on the broader
471 background wind field, its temporal and vertical resolutions limit its ability to resolve
472 localized shear maxima and their rapid evolution immediately preceding rainfall.

473 In summary, despite potential variations in the underlying processes across regions
474 and rainfall regimes, the contrasting evolution of shear magnitude, altitude, and
475 hodograph structure reveals distinct pre-rainfall dynamic characteristics associated with
476 HR and non-HR events. These results demonstrate that the RWP-derived dataset
477 resolves fine-scale and continuous changes in low-level wind shear that are
478 substantially smoothed in ERA5, providing an observational basis for investigating pre-
479 rainfall dynamic environments and evaluating potential shear-based indicators.

480

https://doi.org/10.5194/essd-2026-866
Preprint. Discussion started: 4 November 2026
© Author(s) 2026. CC BY 4.0 License.



4. Data availability

The high-resolution VWS dataset derived from the radar wind profiler network across China is publicly available at https://doi.org/10.5281/zenodo.23432237 (Li and Guo, 2026). ERA5 hourly data are available through the Copernicus Climate Change Service Climate Data Store at https://doi.org/10.24381/cds.bd0915c6 (Hersbach et al., 2023). Automatic weather station measurements were obtained after registration from the National Meteorological Information Center of the China Meteorological Administration (https://data.cma.cn/).

5. Summary and concluding remarks

To address the lack of continuous, fine-scale observations of pre-rainfall dynamic environments, this study develops a high-resolution dataset of low-level VWS derived from 28 RWP stations across China during 2023–2025, covering the 2 h preceding rainfall onset. The dataset provides bulk VWS, layer-mean VWS, maximum VWS, and the altitude of maximum shear at 6 min temporal and 120 m vertical resolutions over 0.6–4.08 km AGL. Comparisons with collocated radiosonde observations show good agreement in the magnitude and vertical structure of VWS, supporting the reliability of the derived dataset. By resolving vertically localized shear maxima and their rapid temporal variations, the dataset complements conventional sounding observations and reanalysis products for characterizing the evolving low-level wind field preceding rainfall.

Using this dataset, we investigated the fine-scale vertical structure and continuous evolution of VWS preceding HR and non-HR events. The observations reveal distinct pre-rainfall dynamic characteristics that cannot be adequately described by background shear magnitude alone. Non-HR events generally exhibit stronger but relatively quasi-steady background VWS, with hodographs dominated by nearly unidirectional shear, whereas HR events show a pronounced nonlinear intensification of low-level VWS beginning approximately 30 min before rainfall onset. This enhancement is most evident in maximum VWS and is accompanied by an upward shift in the mean altitude

https://doi.org/10.5194/essd-2026-866
Preprint. Discussion started: 4 November 2026
© Author(s) 2026. CC BY 4.0 License.



of maximum VWS during the final pre-onset stage. In contrast, the 0.6–3.0 km bulk VWS remains nearly unchanged, indicating that the rapid shear intensification is concentrated within specific altitude layers. The HR hodographs also exhibit greater curvature and a rapid increase in the meridional wind component approaching rainfall onset, reflecting changes in both directional shear and low-level wind structure. These contrasting features indicate that the rapid intensification and vertical redistribution of VWS provide information for distinguishing HR and non-HR pre-rainfall environments beyond background shear magnitude alone.

Comparison with ERA5 further demonstrates the added value of high-resolution RWP observations for resolving fine-scale shear structures. Although ERA5 broadly captures the background wind field and bulk VWS, it underestimates localized maximum VWS and layer-mean VWS, exhibits a downward bias in the altitude of maximum shear, and does not reproduce the rapid temporal variations observed immediately before rainfall onset. The differences are particularly evident for localized shear maxima and the evolving low-level hodograph structure. These discrepancies illustrate the limitations of coarser-resolution reanalysis products for characterizing transient, vertically heterogeneous wind shear and highlight the value of continuous RWP measurements for examining pre-rainfall dynamic environments.

In summary, the RWP-derived VWS dataset provides an observational resource for investigating the fine-scale structure and rapid evolution of the low-level wind field before rainfall. Its high temporal and vertical resolutions offer opportunities to examine pre-convective dynamic processes, evaluate wind-shear representation in numerical models and reanalysis products, and explore potential indicators relevant to regional HR nowcasting. Nevertheless, the lowest observational level of 0.6 km AGL limits characterization of near-surface shear, and the spatial coverage remains constrained by the distribution of RWP stations. Future studies could integrate complementary observations, such as Doppler wind lidar measurements, to extend vertical coverage toward the surface and to investigate the influence of topography, urban environments, and regional circulation patterns on VWS variability. The publicly available dataset

https://doi.org/10.5194/essd-2026-866
Preprint. Discussion started: 4 November 2026
© Author(s) 2026. CC BY 4.0 License.



539 therefore provides a foundation for future research on pre-rainfall dynamical
540 environments and convective-weather monitoring and nowcasting.

541

542 **Author contributions**

543 NL and JG designed the research framework and conceptualized this study. NL,
544 JG and YZ conducted the experiment and drafted the initial manuscript. HX and TC
545 helped the data collection and carried out the quality control. JG, HY, XC, LZ, LZ, XG
546 and TC contributed to the revision of the manuscript. All authors participated in result
547 interpretation.

548 **Competing interests**

549 The contact author has declared that none of the authors has any competing
550 interests.

551 **Disclaimer**

552 Publisher's note: Copernicus Publications remains neutral with regard to
553 jurisdictional claims made in the text, published maps, institutional affiliations, or any
554 other geographical representation in this paper. While Copernicus Publications makes
555 every effort to include appropriate place names, the final responsibility lies with the
556 authors.

557 **Acknowledgements**

558 We thank the editor and anonymous reviewers for their constructive comments
559 and suggestions, which helped improve the manuscript. We also gratefully
560 acknowledge the China Meteorological Administration (CMA) for maintaining the
561 national radar wind profiler network and providing the high-resolution observational
562 data, including radiosonde and rain-gauge measurements, that supported this research.

https://doi.org/10.5194/essd-2026-866
Preprint. Discussion started: 4 November 2026
© Author(s) 2026. CC BY 4.0 License.



Financial support

This work was conceived jointly under the auspices of the National Natural Science Foundation of China (grant no. 42325501), Henan Provincial Major Industrial Key Technology Tackling Project under grant 261000320600, Anhui Provincial Science and Technology Tackling Plan (grant no. 202523t06050001), the Department of Science and Technology of Guizhou province under Grant KXJZ [2024] 033 and [2026] Major 009, and Chinese Academy of Meteorological Science under grants 2026Z001, 2026Z004 and 2024Z003.

https://doi.org/10.5194/essd-2026-866
Preprint. Discussion started: 4 November 2026
© Author(s) 2026. CC BY 4.0 License.



References

Aiyyer, A. R. and Thorncroft, C.: Climatology of vertical wind shear over the tropical Atlantic, J. Clim., 19, 2969–2983, https://doi.org/10.1175/JCLI3736.1, 2006.

Alfaro, D. A.: Low-tropospheric shear in the structure of squall lines: Impacts on latent heating under layer-lifting ascent, J. Atmos. Sci., 74, 229–248, https://doi.org/10.1175/JAS-D-16-0168.1, 2017.

Angevine, W. M.: Errors in mean vertical velocities measured by boundary layer wind profilers, J. Atmos. Ocean. Technol., 14, 565–569, https://doi.org/10.1175/1520-0426(1997)014<0565:EIMVVM>2.0.CO;2, 1997.

Augros, C., Tabary, P., Anquez, A., Moisselin, J., Brovelli, P., and Bousquet, O.: Development of a nationwide, low-level wind shear mosaic in France, Wea. Forecasting, 28, 1241–1260, https://doi.org/10.1175/WAF-D-12-00115.1, 2013.

Barton, E. J., Klein, C., Taylor, C. M., Marsham, J., Parker, D. J., Maybee, B., Feng, Z., and Leung, L. R.: Soil moisture gradients strengthen mesoscale convective systems by increasing wind shear, Nat. Geosci., 18, 1–9, https://doi.org/10.1038/s41561-025-01666-8, 2025.

Cao, Q., Guo, J., Xue, C., Li, Z., Xu, H., Li, N., Sun, Y., Zhang, Z., Wang, Y., Chen, J., Zhou, Y., and Chen, T.: Divergent sounding-derived precursor pathways enable discrimination of dry versus wet severe convective winds, Geophys. Res. Lett., 52, e2025GL117491, https://doi.org/10.1029/2025GL117491, 2025.

Carbone, R. E. and Tuttle, J. D.: Rainfall occurrence in the US warm season: The diurnal cycle, J. Clim., 21, 4132–4146, https://doi.org/10.1175/2008JCLI2275.1, 2008.

Chen, Q., Fan, J., Hagos, S., Gustafson Jr., W. I., and Berg, L. K.: Roles of wind shear at different vertical levels: Cloud system organization and properties, J. Geophys. Res.-Atmos., 120, 6551–6574, https://doi.org/10.1002/2015JD023253, 2015.

Chen, T., Guo, J., Guo, X., Zhang, Y., Xu, H., and Zhang, D.-L.: On the multiscale processes leading to an extreme gust wind event in East China: Insights from radar wind profiler mesonet observations, J. Geophys. Res.-Atmos., 129, e2024JD041484, https://doi.org/10.1029/2024JD041484, 2024.

https://doi.org/10.5194/essd-2026-866
Preprint. Discussion started: 4 November 2026
© Author(s) 2026. CC BY 4.0 License.



602 China Meteorological Administration: Specification for Automatic Observation of
603 Ground Meteorology, China Meteorological Press, Beijing, China, 2020 (in
604 Chinese).
605 Coniglio, M. C., Stensrud, D. J., and Wicker, L. J.: Effects of upper-level shear on the
606 structure and maintenance of strong quasi-linear mesoscale convective systems, J.
607 Atmos. Sci., 63, 1231–1252, https://doi.org/10.1175/jas3681.1, 2006.
608 Draxl, C., Hahmann, A. N., Peña, A., and Giebel, G.: Evaluating winds and vertical
609 wind shear from Weather Research and Forecasting model forecasts using seven
610 planetary boundary layer schemes, Wind Energy, 17, 39–55,
611 https://doi.org/10.1002/we.1555, 2014.
612 Fitzpatrick, R. G. J., Parker, D. J., Marsham, J. H., Rowell, D. P., Guichard, F. M.,
613 Taylor, C. M., Cook, K. H., Vizy, E. K., Jackson, L. S., Finney, D., Crook, J.,
614 Stratton, R., and Tucker, S.: What drives the intensification of mesoscale
615 convective systems over the West African Sahel under climate change?, J. Clim.,
616 33, 3151–3172, https://doi.org/10.1175/JCLI-D-19-0380.1, 2020.
617 Fovell, R. G. and Ogura, Y.: Effect of vertical wind shear on numerically simulated
618 multicell storm structure, J. Atmos. Sci., 46, 3144–3176,
619 https://doi.org/10.1175/1520-0469(1989)046<3144:EOVWSO>2.0.CO;2, 1989.
620 Frank, W. M. and Ritchie, E. A.: Effects of vertical wind shear on the intensity and
621 structure of numerically simulated hurricanes, Mon. Wea. Rev., 129, 2249–2269,
622 https://doi.org/10.1175/1520-0493(2001)129<2249:EOVWSO>2.0.CO;2, 2001.
623 Fu, S. M., Jin, S. L., Shen, W., Li, D. Y., Liu, B., and Sun, J. H.: A kinetic energy budget
624 on the severe wind production that causes a serious state grid failure in Southern
625 Xinjiang China, Atmos. Sci. Lett., 21, e977, https://doi.org/10.1002/asl.977, 2020.
626 Glickman, T. S.: Glossary of Meteorology, 2nd Edn., American Meteorological Society,
627 Boston, MA, USA, 855 pp., 2000.
628 Guo, J., Liu, B., Gong, W., Shi, L., Zhang, Y., Ma, Y., Zhang, J., Chen, T., Bai, K.,
629 Stoffelen, A., de Leeuw, G., and Xu, X.: Technical note: First comparison of wind
630 observations from ESA's satellite mission Aeolus and ground-based radar wind

https://doi.org/10.5194/essd-2026-866
Preprint. Discussion started: 4 November 2026
© Author(s) 2026. CC BY 4.0 License.

profiler network of China, Atmos. Chem. Phys., 21, 2945–2958, https://doi.org/10.5194/acp-21-2945-2021, 2021.

Guo, X., Guo, J., Zhang, D.-L., and Yun, Y.: Vertical divergence profiles as detected by two wind-profiler mesonets over East China: Implications for nowcasting convective storms, Q. J. R. Meteorol. Soc., 149, 1629–1649, https://doi.org/10.1002/qj.4474, 2023.

Hande, L. B., Siems, S. T., Manton, M. J., and Belusic, D.: Observations of wind shear over the Southern Ocean, J. Geophys. Res.-Atmos., 117, D12206, https://doi.org/10.1029/2012JD017488, 2012.

Hersbach, H., Bell, B., Berrisford, P., Hirahara, S., Horányi, A., Muñoz-Sabater, J., Nicolas, J., Peubey, C., Radu, R., Schepers, D., Simmons, A., Soci, C., Abdalla, S., Abellan, X., Balsamo, G., Bechtold, P., Biavati, G., Bidlot, J., Bonavita, M., De Chiara, G., Dahlgren, P., Dee, D., Diamantakis, M., Dragani, R., Flemming, J., Forbes, R., Fuentes, M., Geer, A., Haimberger, L., Healy, S., Hogan, R. J., Hólm, E., Janisková, M., Keeley, S., Laloyaux, P., Lopez, P., Lupu, C., Radnoti, G., de Rosnay, P., Rozum, I., Vamborg, F., Villaume, S., and Thépaut, J. N.: The ERA5 global reanalysis, Q. J. R. Meteorol. Soc., 146, 1999–2049, https://doi.org/10.1002/qj.3803, 2020.

Houchi, K., Stoffelen, A., Marseille, G. J., and De Kloe, J.: Comparison of wind and wind shear climatologies derived from high-resolution radiosondes and the ECMWF model, J. Geophys. Res.-Atmos., 115, D22123, https://doi.org/10.1029/2009JD013196, 2010.

Ko, H. C. and Chun, H. Y.: Increasing trend of vertical wind shear revealed by high-resolution radiosonde data over the United States, npj Clim. Atmos. Sci., 9, https://doi.org/10.1038/s41612-026-01466-w, 2026.

Li, N. and Guo, J.: A high-resolution radar wind profiler-derived dataset of low-level wind shear preceding rainfall across China, Zenodo [data set], https://doi.org/10.5281/zenodo.23432237, 2026.

Li, N., Guo, J., Wu, M., Zhang, F., Guo, X., Sun, Y., Zhang, Z., Liang, L., and Chen, T.: Low-level jet and its effect on the onset of summertime nocturnal rainfall in

https://doi.org/10.5194/essd-2026-866
Preprint. Discussion started: 4 November 2026
© Author(s) 2026. CC BY 4.0 License.



661 Beijing, Geophys. Res. Lett., 51, e2024GL110840,
662 https://doi.org/10.1029/2024GL110840, 2024.
663 Li, N., Guo, J., Guo, X., Chen, T., Zhang, Z., Tang, N., Wang, Y., Yang, H., Zheng, Y.,
664 and Zhou, Y.: On the nationwide variability of low-level jets prior to warm-season
665 nocturnal rainfall in China revealed by radar wind profilers, Atmos. Chem. Phys.,
666 26, 3339–3356, 2026.
667 Liu, B., Ma, Y., Guo, J., and Wei, G.: Boundary layer heights as derived from ground-
668 based radar wind profiler in Beijing, IEEE Trans. Geosci. Remote Sens., 57, 8095–
669 8104, https://doi.org/10.1109/TGRS.2019.2918301, 2019.
670 Liu, S., Zheng, Y., and Tao, Z.: The analysis of the relationship between pulse of LLJ
671 and heavy rain using wind profiler data, J. Trop. Meteorol., 2, 158–163, 2003 (in
672 Chinese).
673 Luo, Y., Gong, Y., and Zhang, D.-L.: Initiation and organizational modes of an extreme-
674 rain-producing mesoscale convective system along a mei-yu front in East China,
675 Mon. Wea. Rev., 142, 203–221, https://doi.org/10.1175/MWR-D-13-00111.1,
676 2014.
677 Markowski, P. and Richardson, Y.: Observations of vertical wind shear heterogeneity
678 in convective boundary layers, Mon. Wea. Rev., 135, 843–861,
679 https://doi.org/10.1175/MWR3334.1, 2007.
680 Maybee, B., Marsham, J. H., Klein, C. M., Parker, D. J., Barton, E. J., Taylor, C. M.,
681 and Warner, J.: Wind shear effects in convection-permitting models influence
682 MCS rainfall and forcing of tropical circulation, Geophys. Res. Lett., 51,
683 e2024GL110119, https://doi.org/10.1029/2024GL110119, 2024.
684 Molod, A., Salmun, H., and Collow, A. B. M.: Annual cycle of planetary boundary layer
685 heights estimated from wind profiler network data, J. Geophys. Res.-Atmos., 124,
686 6207–6221, https://doi.org/10.1029/2018JD030102, 2019.
687 Mulholland, J. P., Peters, J. M., and Morrison, H.: How does vertical wind shear
688 influence entrainment in squall lines?, J. Atmos. Sci., 78, 1931–1946,
689 https://doi.org/10.1175/JAS-D-20-0299.1, 2021.

https://doi.org/10.5194/essd-2026-866
Preprint. Discussion started: 4 November 2026
© Author(s) 2026. CC BY 4.0 License.



690 Reif, D. Q. and Bluestein, H. B.: A 20-year climatology of nocturnal convection
691 initiation over the central and southern Great Plains during the warm season, Mon.
692 Wea. Rev., 145, 1615–1639, https://doi.org/10.1175/MWR-D-16-0340.1, 2017.
693 Roots, M., Sullivan, J. T., and Demoz, B.: Mid-Atlantic nocturnal low-level jet
694 characteristics: a machine learning analysis of radar wind profiles, Atmos. Meas.
695 Tech., 18, 1269–1282, https://doi.org/10.5194/amt-18-1269-2025, 2025.
696 Rotunno, R., Klemp, J. B., and Weisman, M. L.: A theory for strong, long-lived squall
697 lines, J. Atmos. Sci., 45, 463–485, https://doi.org/10.1175/1520-
698 0469(1988)045<0463:atfsll>2.0.co;2, 1988.
699 Stensrud, D. J., Coniglio, M. C., Davies-Jones, R. P., and Evans, J. S.: Comments on
700 "A theory for strong, long-lived squall lines" revisited, J. Atmos. Sci., 62, 2989–
701 2996, https://doi.org/10.1175/jas3514.1, 2005.
702 Takemi, T.: Impacts of moisture profile on the evolution and organization of midlatitude
703 squall lines under various shear conditions, Atmos. Res., 82, 37–54,
704 https://doi.org/10.1016/j.atmosres.2005.01.007, 2006.
705 Taylor, C. M., Belušić, D., Guichard, F., Parker, D. J., Vischel, T., Bock, O., Harris, P.
706 P., Janicot, S., Klein, C., and Panthou, G.: Frequency of extreme Sahelian storms
707 tripled since 1982 in satellite observations, Nature, 544, 475–478,
708 https://doi.org/10.1038/nature22069, 2017.
709 Taylor, C. M., Klein, C., Barton, E. J., Hahn, S., and Wagner, W.: Wind shear enhances
710 soil moisture influence on rapid thunderstorm growth, Nature, 651, 116–121,
711 https://doi.org/10.1038/s41586-025-10045-7, 2026.
712 Trier, S. B., Davis, C. A., Ahijevych, D. A., Weisman, M. L., and Bryan, G. H.:
713 Mechanisms supporting long-lived episodes of propagating nocturnal convection
714 within a 7-day WRF model simulation, J. Atmos. Sci., 63, 2437–2461,
715 https://doi.org/10.1175/JAS3768.1, 2006.
716 Wang, L., Wang, G., Gu, Y., Li, H., Ma, L., Guo, J., and Qiao, L.: Application of wind
717 profiler radar vertical radial velocity, Meteor. Mon., 40, 290–296,
718 https://doi.org/10.7519/j.issn.1000-0526.2014.03.004, 2014 (in Chinese).

https://doi.org/10.5194/essd-2026-866
Preprint. Discussion started: 4 November 2026
© Author(s) 2026. CC BY 4.0 License.



719 Weisman, M. L., Trapp, R. J., Romine, G. S., Davis, C., Torn, R., Baldwin, M., Bosart,
720 L., Brown, J., Coniglio, M., Dowell, D., Evans, A. C., Galarneau, T. J., Haggerty,
721 J., Hock, T., Manning, K., Roebber, P., Romashkin, P., Schumacher, R., Schwartz,
722 C. S., Sobash, R., Stensrud, D., and Trier, S. B.: The mesoscale predictability
723 experiment (MPEX), Bull. Am. Meteorol. Soc., 96, 2127–2149,
724 https://doi.org/10.1175/bams-d-13-00281.1, 2015.
725 Xue, Y., He, J., Chan, P., and Li, Q.: Multi-source observational study of wind shear
726 and veer at Hong Kong International Airport, Urban Clim., 65, 102758,
727 https://doi.org/10.1016/j.uclim.2025.102758, 2026.
728 Zamora, R. J., Shapiro, M. A., and Doswell III, C. A.: The diagnosis of upper
729 tropospheric divergence and ageostrophic wind using profiler wind observations,
730 Mon. Wea. Rev., 115, 871–884, https://doi.org/10.1175/1520-
731 0493(1987)115<0871:TDOUTD>2.0.CO;2, 1987.
732 Zhang, H., Wu, S., Wang, Q., Liu, B., and Zhai, X.: Airport low-level wind shear lidar
733 observation at Beijing Capital International Airport, Infrared Phys. Technol., 96,
734 113–122, https://doi.org/10.1016/j.infrared.2018.07.033, 2019.
735 Zhang, Y., Guo, J., Yang, Y., Wang, Y., and Yim, S. H. L.: Vertical wind shear modulates
736 particulate matter pollutions: A perspective from radar wind profiler observations
737 in Beijing, China, Remote Sens., 12, 546, https://doi.org/10.3390/rs12030546,
738 2020.
739 Zhao, Y., Liao, J., Zhang, Q., Chen, J., Gong, X., Shi, Y., Shi, M., Yang, D., Fan, S.,
740 Zhou, X., Cao, L., and Hu, K.: Development of China ground climate normal value
741 dataset from 1991 to 2020, Chinese J. Atmos. Sci., 48, 555–571,
742 https://doi.org/10.3878/j.issn.1006-9895.2204.22010, 2024 (in Chinese).
743 Zheng, L. and Sun, J.: The impact of vertical wind shear on the intensity and
744 organizational mode of mesoscale convective systems using numerical
745 experiments, Chinese J. Atmos. Sci., 40, 324–340, 2016 (in Chinese).
746